The EHD protein Past1 controls postsynaptic membrane elaboration and synaptic function

Kate Koles[a], Emily M. Messelaar[a], Zachary Feiger[a], Crystal J. Yu[a], C. Andrew Frank[b], and Avital A. Rodal[a]

[a]Rosenstiel Basic Medical Sciences Research Center, Department of Biology, Brandeis University, Waltham, MA 02453; [b]Department of Anatomy and Cell Biology, University of Iowa, Iowa City, IA 52242

ABSTRACT **Membranes form elaborate structures that are highly tailored to their specialized cellular functions, yet the mechanisms by which these structures are shaped remain poorly understood. Here, we show that the conserved membrane-remodeling C-terminal Eps15 Homology Domain (EHD) protein Past1 is required for the normal assembly of the subsynaptic muscle membrane reticulum (SSR) at the *Drosophila melanogaster* larval neuromuscular junction (NMJ). *past1* mutants exhibit altered NMJ morphology, decreased synaptic transmission, reduced glutamate receptor levels, and a deficit in synaptic homeostasis. The membrane-remodeling proteins Amphiphysin and Syndapin colocalize with Past1 in distinct SSR subdomains and collapse into Amphiphysin-dependent membrane nodules in the SSR of *past1* mutants. Our results suggest a mechanism by which the coordinated actions of multiple lipid-binding proteins lead to the elaboration of increasing layers of the SSR and uncover new roles for an EHD protein at synapses.**

Monitoring Editor
Patricía Bassereau
Institut Curie

Received: Feb 18, 2015
Revised: Jun 24, 2015
Accepted: Jul 14, 2015

INTRODUCTION

Dozens of lipid-binding proteins dynamically remodel membranes, generating diverse cell shapes, sculpting organelles, and promoting traffic between subcellular compartments. Although the activities of many of these membrane-remodeling proteins have been studied individually, what is lacking is an understanding of how membrane-remodeling factors work together to generate specialized membranes in vivo.

C-terminal Eps15 Homology Domain (EHD)–family proteins encode large membrane-binding ATPases with structural similarity to dynamin and function at a variety of steps of membrane transport (Naslavsky and Caplan, 2011). These proteins contain an ATPase domain, a helical lipid-binding domain, and a carboxy-terminal EH domain that interacts with Asn-Pro-Phe (NPF)–containing binding partners (Naslavsky and Caplan, 2011). Although their mechanism of action is not fully understood, it is postulated that C-terminal EHD proteins bind and oligomerize in an ATP-dependent manner on membrane compartments, where they are involved in the trafficking of cargo (Grant *et al.*, 2001; Lin *et al.*, 2001; Lee *et al.*, 2005; Daumke *et al.*, 2007). The mouse and human genomes each contain four highly similar EHD proteins (EHD1–4), which have both unique and overlapping functions (Naslavsky and Caplan, 2011). EHD proteins interact with several members of the Bin/Amphiphysin/Rvs167 (BAR) and Fes/Cip4 homology-BAR (F-BAR) protein families, which themselves can remodel membranes via their crescent-shaped dimeric BAR domains (Masuda and Mochizuki, 2010). In mammals, EHD proteins associate with the NPF motifs of the F-BAR proteins Syndapin I and II, and these interactions are critical for recycling of cargo from endosomes to the plasma membrane in cultured cells (Xu *et al.*, 2004; Braun *et al.*, 2005). In *Caenorhabditis elegans*, the sole EHD protein Rme-1 colocalizes and functions with the BAR protein Amphiphysin and the F-BAR protein Syndapin, also via their NPF motifs (Pant *et al.*, 2009). Further, EHD1 has been suggested to drive the scission of endosomal recycling tubules generated by the membrane-deforming activities of Syndapin 2 and another NPF-containing protein, MICAL-L1 (Giridharan *et al.*, 2013). However, the combined membrane-remodeling activities that might arise in vivo from the shared functions of C-terminal EHD and NPF-containing proteins remain unclear.

The *Drosophila* neuromuscular junction (NMJ) is a powerful system in which to study membrane remodeling. On the postsynaptic

This article was published online ahead of print in MBoC in Press (http://www.molbiolcell.org/cgi/doi/10.1091/mbc.E15-02-0093) on July 22, 2015.

Address correspondence to: Avital A. Rodal (arodal@brandeis.edu).

Abbreviations used: BAR, Bin/Amphiphysin/Rvs167; EHD, Eps15-homology domain; F-BAR, Fes/Cip4-homology-Bin/Amphiphysin/Rvs167; FRAP, fluorescence recovery after photobleaching; NA, numerical aperture; NMJ, neuromuscular junction; NPF, Asp-Pro-Phe; SSR, subsynaptic reticulum; TEM, transmission electron microscopy.

side of the NMJ, a highly convoluted array of muscle membrane infoldings called the subsynaptic reticulum (SSR) incorporates neurotransmitter receptors, ion channels, and cell adhesion molecules. Assembly of the SSR during larval growth involves activity-dependent targeted exocytosis mediated by the small GTPase Ral and its effector, the exocyst complex (Teodoro *et al.*, 2013), as well as the t-SNARE (target soluble *N*-ethylmaleimide–sensitive factor attachment protein receptor) receptor gtaxin/Syx18 (Gorczyca *et al.*, 2007) and scaffolding proteins such as Discs Large (Dlg; Lahey *et al.*, 1994). Many proteins with predicted membrane-remodeling activities, including *Drosophila* homologues of Syndapin (Synd) and Amphiphysin (Amph), localize extensively to SSR membranes, making them prime candidates to facilitate SSR elaboration (Leventis *et al.*, 2001; Razzaq *et al.*, 2001; Zelhof *et al.*, 2001; Kumar *et al.*, 2009b). Amph regulates the postsynaptic turnover of the trans-synaptic cell adhesion molecule FasII (Mathew *et al.*, 2003), but its role in organizing the SSR is unknown.

The *Drosophila melanogaster* genome encodes a single C-terminal EHD protein called Putative achaete/scute target (Past1). Past1 mutants exhibit defects in endocytic recycling in larval nephrocytes, sterility and aberrant development of the germline, and short lifespan (Olswang-Kutz *et al.*, 2009), but the functions of Past1 at the NMJ have not been explored. Mammalian EHD1 localizes to the mouse NMJ, but its function there has been difficult to ascertain, perhaps due to redundancy with other EHD proteins (Mate *et al.*, 2012). Here we take advantage of the fact that Past1 encodes the only *Drosophila* C-terminal EHD protein and define its role at the NMJ.

RESULTS

Past1 localizes to the SSR and is required for proper SSR assembly

We first investigated a potential role for Past1 in the neuromuscular system by examining its localization at the larval NMJ relative to the neuronal membrane marker anti–horseradish peroxidase (α-HRP) and the presynaptic and postsynaptic scaffolding protein Dlg. Larval muscles are innervated by glutamatergic type Ib NMJs (which are surrounded by extensive SSR and Dlg), glutamatergic type Is NMJs (which are surrounded by a much thinner layer of SSR and Dlg), and peptidergic type II and III NMJs (which lack both SSR and Dlg; Prokop, 2006). Polyclonal α-Past1 antibodies (Olswang-Kutz *et al.*, 2009) revealed endogenous Past1 localization at the NMJ to type Ib and Is arbors but not to type II or type III arbors (Figure 1A), suggesting that Past1 localizes specifically to SSR-surrounded NMJs. Past1 localized to a postsynaptic domain larger than that defined by Dlg and decorated frequent tubule-like extensions into the muscle (Figure 1B, arrows). This Past1 immunolabeling disappeared in *past1*-null mutants and was lost after postsynaptic depletion of Past1 by RNA interference (RNAi), confirming the specificity of the labeling (Figure 1C). Localization of Past1 to the SSR was recapitulated using a Past1–enhanced green fluorescent protein (EGFP) transgene driven by the muscle driver BG487-GAL4 (Figure 1D). By contrast, the mutant Past1^{G62E}-EGFP protein (analogous to mutations in mammalian and *C. elegans* EHD1/*rme*-1, which abolish ATP binding and membrane association; Lee *et al.*, 2005) was diffusely localized in the muscle, with only a small degree of enrichment at the NMJ (Figure 1D), indicating that ATP binding and membrane binding by Past1 are required for its localization.

Past1 also localized to tubulovesicular structures in the muscle cortex (Figure 1B and Supplemental Figure S1A) and to Dlg-labeled muscle–muscle junctions. Of interest, however, it did not localize to t-tubules, which are prominent deep invaginations of the muscle plasma membrane that couple muscle membrane depolarization to calcium release from the sarcoplasmic reticulum and also contain Dlg (Razzaq *et al.*, 2001; Supplemental Figure S1A). Finally, whereas muscle-specific RNAi revealed negligible expression of Past1 in the motor neuron (Figure 1C), ectopic presynaptic expression of Past1-EGFP induced the formation of extensive tubules emanating from the presynaptic arbor, consistent with Past1 having a robust membrane deformation activity. These tubules contained presynaptic membrane marker HRP but were not enriched for the presynaptic proteins we tested (Supplemental Figure S1B), suggesting that they exclude presynaptic cytoplasm and ultrastructures.

Given the localization of Past1 to the NMJ and its expected role in membrane remodeling, we next examined the morphology of this synapse in *past1*$^{60\text{-}4/110\text{-}1}$-null mutants (Olswang-Kutz *et al.*, 2009). Whereas total bouton number was similar to that for wild-type animals (Figure 1E and Supplemental Table S1), *past1* mutants exhibited a marked defect in synaptic bouton shape. Boutons were less round than wild-type boutons, often with ragged edges (Figure 1E). We also found a significant increase in the frequency of ghost boutons (Figure 1, F and G), defined by the dramatic reduction or absence of a postsynaptic marker (Dlg) at α-HRP–labeled type Ib and type Is boutons on muscles 6 and 7, which are particularly sensitive to this phenotype (Ataman *et al.*, 2008). However, the amount of postsynaptically localized α-HRP labeling (representing shed neuronal membrane debris; Fuentes-Medel *et al.*, 2009) was similar in wild type and *past1* mutants, suggesting that ghost boutons did not arise from excessive presynaptic membrane shedding (Figure 1H). The NMJ morphology and ghost bouton phenotype were rescued by reexpression of Past1-EGFP in muscles (Figure 1, E–G). Therefore Past1 is required postsynaptically for normal synaptic morphogenesis.

Past1 is required for synaptic transmission and homeostasis

To test the effects of Past1 on NMJ function, we next examined synaptic transmission in *past1* mutants. The larval NMJs to which Past1 localizes are glutamatergic synapses and depend on a glutamate receptor (GluR) tetramer consisting of the invariant subunits GluRIIC, GluRIID, and GlurIIE and the variable subunits GluRIIA and GluRIIB, which determine the electrophysiological properties of the receptor (DiAntonio *et al.*, 1999; Marrus *et al.*, 2004). At the larval NMJ, GluRIIA-containing complexes are believed to represent nascent synapses, whereas GluRIIB complexes are believed to represent more mature, stable synapses (Thomas and Sigrist, 2012). In addition, this NMJ exhibits robust homeostasis in response to reduced activity of glutamate receptors, responding with an increase in presynaptic release dependent on a retrograde signal and Ca^{2+} influx (Petersen *et al.*, 1997; Frank, 2014). To determine the role of Past1 in glutamatergic signaling at the NMJ, we immunostained *past1* mutants with glutamate receptor–specific antibodies and found a specific reduction in the levels of GluRIIA but not of GluRIIB or GluRIIC (Figure 2, A and B). Despite reduced GluRIIA levels, GluRIIC clusters in *past1* mutants were apposed normally to presynaptic active zones marked by Bruchpilot (BRP) (Figure 2C), suggesting that synapse formation was not affected.

We then used electrophysiology to examine the functional consequences of loss of Past1. Compared to controls, *past1*-mutant NMJs exhibited strongly reduced spontaneous miniature excitatory postsynaptic potentials (mEPSPs; Figure 2, D and E), as well as dampened evoked postsynaptic potentials (EPSPs; Figure 2, D and F). The frequency of mEPSPs was also depressed (Figure 2G), perhaps because reduced mEPSP amplitude precludes detection of some events. Strikingly, quantal content was not increased to compensate for mEPSP amplitude reduction (Figure 2H), suggesting a

defect in synaptic homeostasis. To test this possibility, we used the null mutation *GluRIIA*^{SP16}, representing a challenge to postsynaptic function that produces a robust homeostatic response (Petersen *et al.*, 1997). Compared to *past1* single mutants, we found that *past1; GluRIIA*^{SP16} double mutants exhibited a further reduction in mEPSP amplitude (Figure 2, D and E). These mEPSPs in *past1; GluRIIA*^{SP16} mutants were very similar in amplitude to *GluRIIA*^{SP16} single mutants (Figure 2E), suggesting that the reduction in mEPSP amplitude in *past1* mutants is predominantly due to diminished GluRIIA levels. Remarkably, although we observed robust homeostatic compensation in *GluRIIA*^{SP16} single mutants (as evidenced by increased quantal content), *GluRIIA*^{SP16}; *past1* double mutants had the same diminished quantal content as *past1* single mutants (Figure 2H). These results indicate that *past1* mutants have a specific and strong defect in synaptic homeostasis.

Past1 organizes the subsynaptic reticulum

Past1 is a membrane-remodeling protein, and the defects in synaptic morphology, transmission, and homeostasis that we observed may be due to a direct role in organizing postsynaptic membranes. To test the role of Past1 in the SSR, we examined the organization of postsynaptic membranes using a muscle-expressed myristoylated monomeric red fluorescent protein (myr-mRFP, targeted to membranes via fatty acid modification) or mCD8-GFP (targeted to membranes using the transmembrane domain of mouse CD8). Both reporters localized strongly to the SSR in control and *past1*-mutant NMJs but were found partly concentrated in nodules at *past1*-mutant NMJs (Figure 3A, arrows).

Myr-mRFP is predicted to diffuse readily within membranes, so we used it as a reporter for mobility within membranes in the SSR, using fluorescence recovery after photobleaching (FRAP) analysis. At the resolution of light microscopy, myr-mRFP intensity and volume were unchanged between wild-type and *past1*-mutant NMJs (Figure 3B). On photobleaching a string of terminal boutons in either wild-type or past1 mutants, myr-mRFP recovered first in the proximal bouton and last in the distal bouton (Figure 3C, arrows), indicating that membrane diffusion occurs primarily between the SSR of adjacent boutons rather than between the NMJ and the muscle cortex. In *past1* mutants, myr-mRFP exhibited a similar recovery rate but a significantly higher mobile fraction than in wild-type animals, suggesting that the SSR reticulum may have reduced complexity, allowing more extensive membrane exchange (Figure 3C and Supplemental Movies S1 and S2).

To examine further the ultrastructure of the mutant NMJ, we used transmission electron microscopy (TEM). The *past1*-mutant boutons exhibited normal presynaptic structures, including synaptic vesicles and active zones (Figure 3D). TEM of wild-type type 1b boutons revealed a highly elaborated postsynaptic reticulum (Figure 3D). In striking contrast, Past1- mutant type 1b boutons exhibited aberrant SSR membranes, often separated into distinct nodules. Further, a fraction of the nodules (5 of 12 nodules; $n = 5$ boutons) exhibited a central core (yellow arrow) surrounded by long membrane extensions ~20 nm wide in cross section (Figure 3D, red arrow). Nodules were not seen in wild-type samples ($n = 5$ boutons). Because thin tubules would be unlikely to extend so frequently and for such long distances in the plane of the thin section, it is likely that these extensions represent flat membrane sheets. We tested this possibility by conducting serial section electron microscopy on NMJs and indeed found that the long membrane extensions in nodules continued through multiple ~70-nm sections (Figure 3E), consistent with the hypothesis that they represent membrane sheets. These membrane nodules are likely to correspond to the nodules seen by confocal microscopy of the membrane markers mCD8-GFP and myr-mRFP (Figure 3A). Thus Past1 is required for normal development and morphology of the SSR.

Past1 functionally interacts with Synd and colocalizes with Amph

Synd and Amph are two NPF motif–containing membrane-remodeling proteins that localize to SSR at the *Drosophila* larval NMJ (Leventis *et al.*, 2001; Razzaq *et al.*, 2001; Zelhof *et al.*, 2001; Kumar *et al.*, 2009b) and interact with EHD proteins in other systems (Xu *et al.*, 2004; Braun *et al.*, 2005; Pant *et al.*, 2009). Amph-A is the only one of three *Drosophila* Amphiphysin splice isoforms that contains an NPF motif (Zelhof *et al.*, 2001), whereas all predicted *Drosophila* Synd isoforms contain a single NPF motif (Figure 4A). To test whether Synd and Amph might function with *Drosophila* Past1, we expressed them in cultured *Drosophila* S2 cells. Past1-EGFP localized to tubular and punctate structures in these cells (Figure 4B). By contrast, the ATP-binding mutant Past1^{G62E}-GFP localized primarily to the cytoplasm and infrequent aggregates, whereas Past1 lacking its NPF-interacting EH domain (Past1$^{\Delta EH}$-EGFP) localized primarily to the cytoplasm (Figure 4B). Thus Past1 requires its ATP/membrane-binding capacity as well as its EH domain for localization in S2 cells. Amph-A localized to small puncta, as did an Amph NPF motif mutant in which the conserved EH domain–interacting phenylalanine was replaced with alanine (Figure 4C; Pant *et al.* 2009). The isolated Synd F-BAR domain localized to short tubules and puncta, often emanating in a radial pattern from the center of the cell, whereas full-length Synd localized mainly to the cytoplasm and only weakly to puncta, consistent with previous results demonstrating autoinhibition of the Synd F-BAR by its SH3 domain (Kumar *et al.*, 2009b; Rao *et al.*, 2010; Figure 4D). We mutated the conserved phenylalanine in the NPF motif of Synd to alanine (Synd^{NPFmut}) and found a similar localization to wild-type Synd (Figure 4D).

We first tested the effects of coexpression of Amph and Past1-EGFP in S2 cells. Past1-EGFP colocalized with a fraction of Amph-positive puncta, and this localization was retained when the Amph NPF motif was mutated (Figure 4C). These results suggest that colocalization does not depend on Past1 EH domain–Amph NPF motif interactions, although Past1 and Amph can be recruited to the same cellular structures. We next tested the effects of Past1 on Synd localization. Strikingly, when coexpressed with Past1-EGFP, Synd-mCherry partially relocalized from the cytoplasm to a radial pattern, reminiscent of its isolated F-BAR, and Past1-EGFP colocalized with these structures (Figure 4C). By contrast, Past1-EGFP colocalized significantly less with structures formed by the isolated Synd F-BAR, which is missing the Past1-interacting NPF motif (Figure 4D). Further, the Synd^{NPFmut} mutant exhibited reduced colocalization with Past1 compared with wild-type Synd. These results suggest that in S2 cells, Past1 (either directly or indirectly) interacts with and releases Synd from autoinhibition, revealing a membrane-binding activity similar to its isolated F-BAR. Taken together, these data suggest that functional interactions between Past1 and Synd are likely to be conserved for the *Drosophila* homologues of these proteins. Finally, we found that Past1-EGFP, Synd-mCherry, and Amph-myc colocalized in puncta when expressed together in S2 cells (Supplemental Figure S2), indicating that they can associate with the same structures in vivo.

Past1 organizes distinct SSR domains defined by Amph and Synd

To understand how Past1 sculpts the SSR, we examined its effects on the localization of Amph and Synd at the NMJ. In wild-type

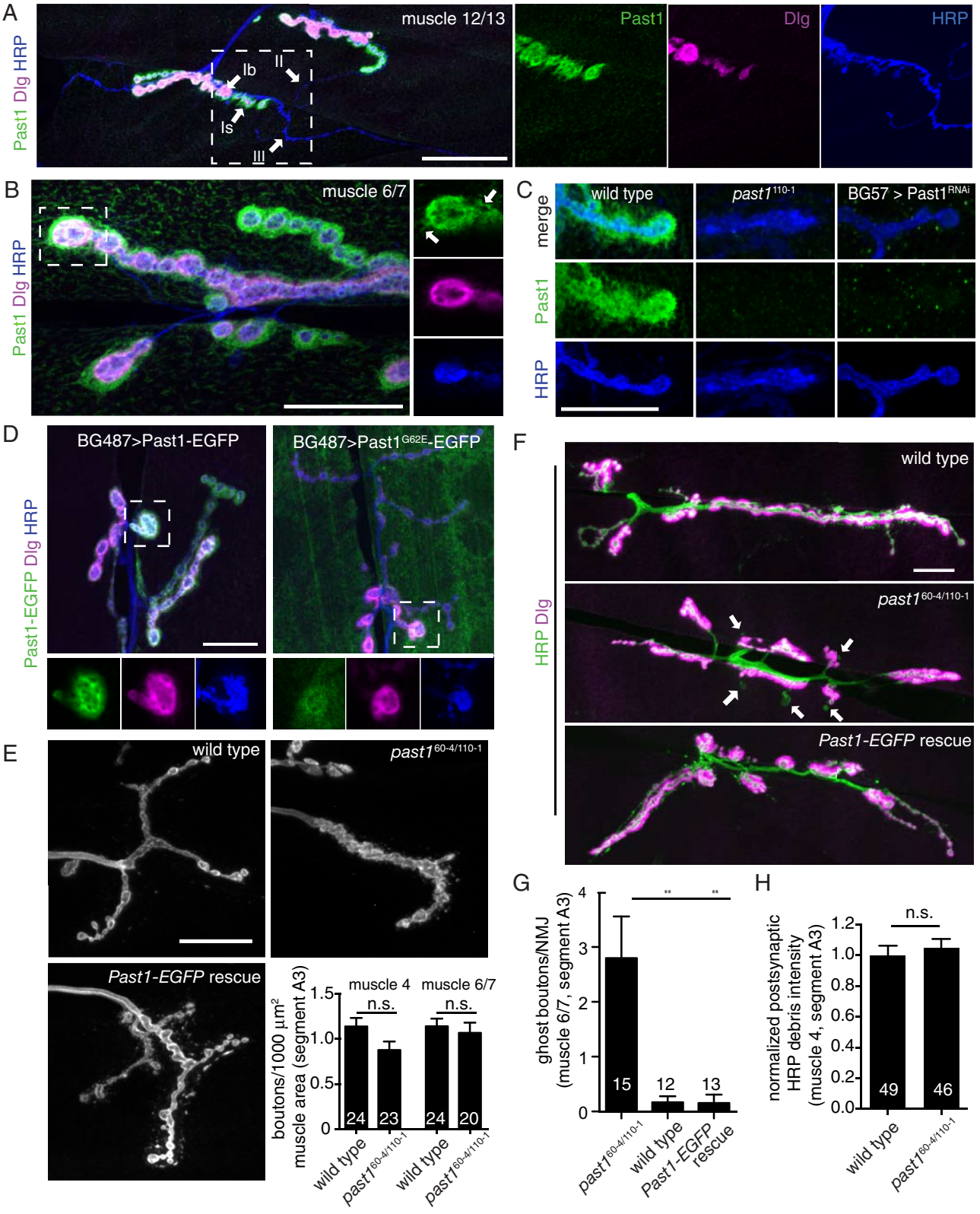

FIGURE 1: Past1 localizes to a postsynaptic tubular-reticular domain at the larval NMJ and is required for postsynaptic membrane assembly. (A) Localization of Past1 to type Ib and Is but not type II or III NMJs. Large image shows 2D projections of 60× spinning-disk confocal stack from an NMJ on muscles 12 and 13. Scale bar, 50 µm. Right, magnified single confocal slices from the area indicated by the dashed rectangle. (B) Large image shows 2D projection of 100× spinning-disk confocal stack from an NMJ on muscles 6 and 7. Right, magnified single confocal slices from the area indicated with the dashed lines; arrows indicate Past1-labeled tubules. (C) NMJ α-Past1 antibody staining is lost in *past1* mutants and upon RNAi of Past1 using the muscle-specific driver BG57-GAL4. Images show 2D projections of 60× spinning-disk confocal stacks from muscle 4. (D) Postsynaptically expressed Past1-EGFP exhibits similar NMJ

animals, Synd and Amph were found at the NMJ in uniformly distributed small postsynaptic puncta (Figure 5A), consistent with previous reports that they colocalize with postsynaptic Dlg (Kumar *et al.*, 2009a,b). However, in *past1*-mutant NMJs, both Synd and Amph were strikingly mislocalized to nodules close to the presynaptic membrane (Figure 5A). Nodules appeared in 82% of *past1*-mutant NMJs (but no wild-type NMJs; Supplemental Figure S3A) and were distinct from the presynaptic active zone marker BRP, which labels synapses (Supplemental Figure S3B). These nodules coincided with indentations of the presynaptic membrane (Figure 5B, arrows) and colocalized strongly with the postsynaptically expressed membrane marker mCD8-GFP (Figure 5C), suggesting that Synd and Amph nodules represent the membrane structures seen by TEM. Further, Synd nodules were recapitulated by RNAi knockdown of Past1 in muscles, indicating that they arise due to lack of postsynaptic Past1 function (Figure 5D). We next tested whether Synd and Amph levels were altered in *past1*-mutant NMJs and found that whereas total levels were unchanged at the NMJ (Figure 5E), there was a higher fraction of Synd- and Amph-positive pixels at higher fluorescence intensities relative to wild-type NMJs, consistent with the observed increased clustering of both Synd and Amph in the nodules (Figure 5F).

We next tested the localization of a number of additional postsynaptic components in *past1* mutants by confocal microscopy. We found that the BAR domain–containing protein dRich (Nahm *et al.*, 2010b) and the F-BAR protein dCip4 (Nahm *et al.*, 2010a) were localized to structures very similar to Synd nodules (Supplemental Figure S3C). The postsynaptic scaffolding molecules Dlg and spectrin, which are not believed to bind to EHD proteins like Past1, were also mislocalized, forming a honeycomb pattern around the NMJ (Supplemental Figure S3D). Thus loss of Past1 causes significant reorganization of postsynaptic membrane-associated and scaffolding proteins.

To understand further the organization of SSR components in *past1* mutants, we used structured illumination microscopy (SIM), with which we could image their organization beyond the diffraction limit of conventional fluorescence microscopy. In wild-type animals, SIM revealed Synd localization in a punctate pattern, along tubules that extended beyond the Dlg domain (Figure 5G), similar to Past1 localization (Figure 1B) and providing increased resolution over previous studies (Kumar *et al.*, 2009a,b). In wild-type animals, Amph localized in small puncta that closely overlapped with the Dlg domain of the SSR (Figure 5G). Thus, in wild-type animals, Synd localizes to a more extensive SSR domain than Amph. By contrast, intensity profiles averaged across multiple *past1*-mutant nodules revealed that Synd localized to the center of the nodule, whereas Amph labeled a region larger than the central domain and Dlg occupied a further domain on the muscle side of the nodule (Figure 5, G and H). Thus the relative positions of Synd and Amph in the SSR are reversed in *past1*-mutant NMJs. These results suggest that the aberrant membrane structures visualized by TEM and mCD8-GFP or myr-mRFP labeling represent a core containing Synd, a larger domain containing Amph (potentially in the membrane sheets we observed by TEM), and a surrounding concentric region containing Dlg.

Finally, we tested the role of Past1 ATP binding/membrane binding in the consolidation of the Synd-labeled membrane domain into nodules. First, we confirmed that postsynaptic reexpression of Past1-EGFP (using the muscle driver BG57-GAL4) in the *past1* mutant rescued the SSR distribution of Synd (Supplemental Figure S4). By contrast, control larvae expressing mCD8-GFP in the *past1*-mutant background exhibited Synd nodules, with which mCD8-GFP colocalized. The ATP/membrane-binding mutant Past1^{G62E}-EGFP failed to rescue the Synd nodule phenotype and localized to the nodules (Supplemental Figure S4). Taken together, our results indicate that ATP/membrane binding by Past1 is required to fully elaborate the SSR and that, in its absence, a membrane domain defined by Amph aberrantly surrounds a domain defined by Synd.

Amph is required to consolidate Synd into nodules

To test the order of action of Amph and Synd microdomains in postsynaptic membrane elaboration, we examined the localization of Synd in *amph*; *past1* double mutants by confocal microscopy. Strikingly, in these double mutants, Synd was no longer localized to nodules but instead was strongly depleted from the NMJ, and its overall levels in the muscle were slightly but significantly reduced (Figure 6, A and B). By contrast, *amph* single mutants had Synd levels similar to those of wild-type NMJs (Figure 6, A and B). This result suggests that Amph is required to pack Synd into the nodules that form in *past1* mutants and that in the absence of NMJ localization, Synd may be destabilized.

We next used confocal microscopy to assess the localization of Dlg as a proxy for overall SSR organization. Dlg was localized to a slightly but significantly larger domain in *amph* single mutants than in *past1* single mutants (Figure 6, A and C). In contrast to the dramatic mislocalization of Synd, *amph*; *past1* mutant NMJs did not have significantly different Dlg volume or intensity than wild-type or *past1*-mutant NMJs. This suggests that unpacking of Synd nodules and mislocalization of Synd from the SSR in *amph; past1* mutants are specific to the Synd structure rather than due to a general loss of SSR. Of importance, GluRIIA levels were similar in *amph*; *past1* double mutants compared with *past1* single mutants (Figure 6D), suggesting that loss of GluRIIA is a general property of *past1* mutants and not an indirect effect of Synd nodule formation.

To examine further the phenotype of *amph*; *past1* double mutants, we examined their SSR organization by TEM. The *amph*-mutant SSR had a similar appearance to wild-type SSR (Figure 6E). Further, in contrast to *past1* single-mutant SSR, we did not observe any nodules or concentric membrane sheets in the *amph; past1* double-mutant SSR (Figure 6E). Thus we conclude that in the

localization to endogenous Past1, whereas an ATP-binding mutant (contrast enhanced) is largely cytoplasmic. Large images show 2D projection of 60× spinning-disk confocal stack from an NMJ on muscles 6 and 7. Bottom, magnified single confocal slices from the area indicated by the dashed rectangle. (E) α-HRP staining showing aberrant bouton morphology in *past1* mutants that is rescued by postsynaptic reexpression of Past1-EGFP. Overall bouton number per muscle area is normal in *past1* mutants (muscles 4 and 6/7, segment A3). Image shows 2D projection of 60× spinning-disk confocal stacks from muscle 4. (F) *past1*-mutant NMJs exhibit ghost boutons. Images shows 2D projection of 60× spinning-disk confocal stacks from muscle 6/7, segment A3. (G) Quantification of ghost boutons. (H) Quantification of postsynaptic α-HRP debris from three-dimensional (3D) volumes surrounding presynaptic terminals. Number in bar graphs indicates number of NMJs measured; scale bars, 20 μm (B–F). Past1-EGFP rescue represents the genotype UAS-Past1-EGFP/+; BG57, *past1*$^{110\text{-}1}$/*past1*$^{60\text{-}4}$.

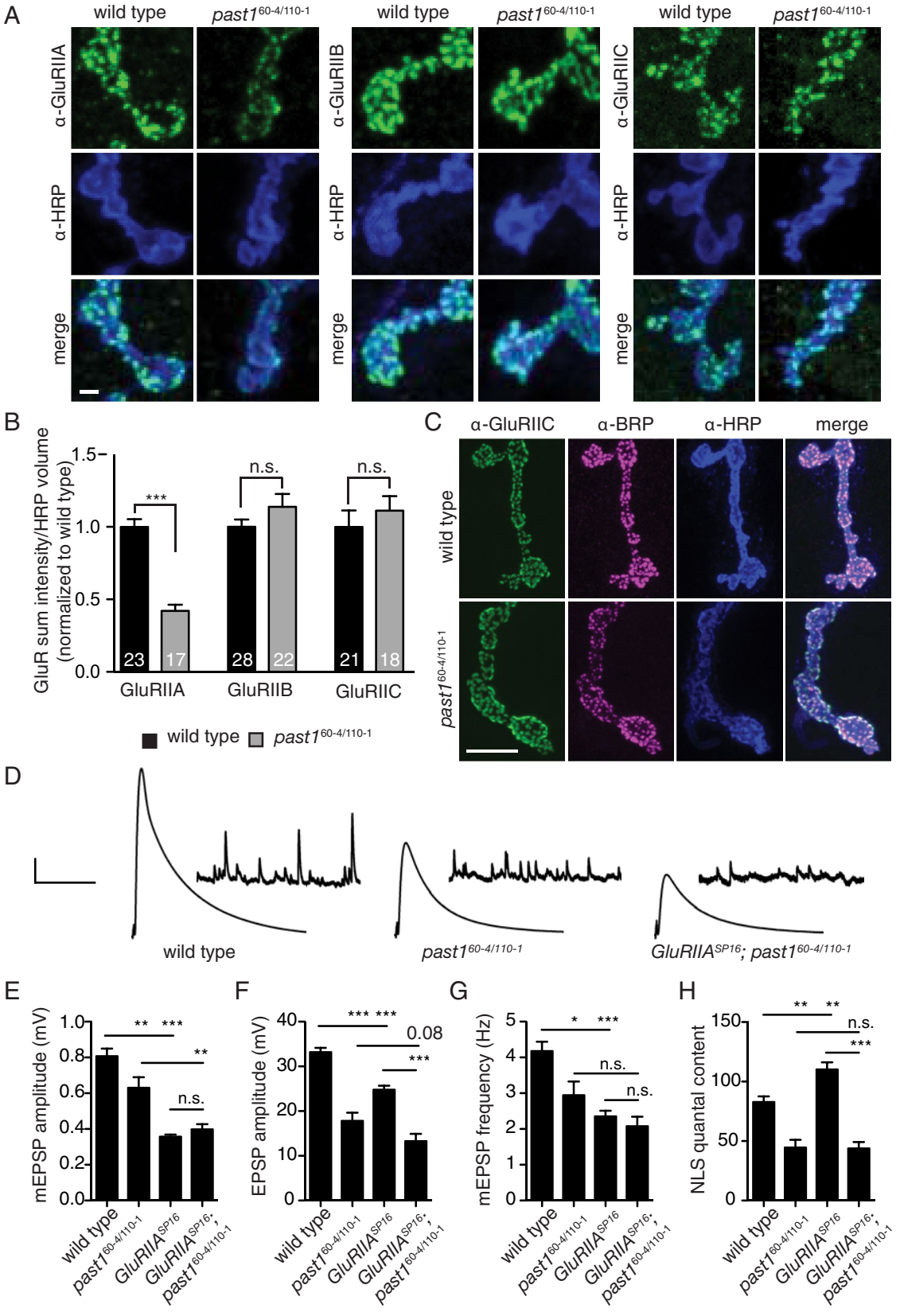

FIGURE 2: Past1 mutants have reduced postsynaptic responses and defective homeostatic compensation. (A) Past1 mutants have reduced GluRIIA levels but normal GluRIIB and GluRIIC levels. Maximum intensity projections of 60× spinning-disk confocal stacks from a representative muscle 4. Scale bar, 2 μm. (B) Quantification of GluR levels from 3D volumes surrounding HRP staining. (C) Normal presynaptic (α-BRP) and postsynaptic (α-GluRIIC) apposition in *past1* mutants. Maximum intensity projections of 100× spinning-disk confocal stacks from a representative muscle 4. Scale bar,

absence of Past1, Amph-dependent membrane sheets are required to consolidate or pack a Synd domain, and these events lead to dysfunctional elaboration of the SSR.

DISCUSSION

Roles of Past1, Synd, and Amph in membrane elaboration

Although there is great diversity in the morphologies of subcellular membranes and organelles, we have relatively little understanding of the mechanisms by which these complex shapes are generated. Here we uncovered novel functional roles in membrane remodeling at the NMJ for Past1, the sole C-terminal EHD protein in *Drosophila*.

Putting together our observations at the NMJ and in S2 cells with previous results from other groups, we propose a new working model for how Past1 functions in synaptic membrane elaboration (Figure 7). Our first key observation is that Past1 is required for normal elaboration of the SSR and that this function depends on its ATP-binding and thus membrane-remodeling activity. Next we found that in wild-type SSR, Amph localizes to a domain proximal to the bouton, whereas Past1 and Synd localize to a more extended tubulovesicular domain. By contrast, in the absence of Past1, the SSR rearranges into highly organized subdomains, with a core of Synd surrounded by a shell of Amph (likely corresponding to membrane sheets seen in Figure 3D by transmission electron microscopy [TEM]). We found that Amph is required for the formation of the sheets (perhaps by regulating the tight curvature at the tips of these membrane structures) and for consolidation of Synd into nodules. Further, our FRAP data indicate that the nodules result in significantly increased membrane flow within the SSR relative to wild-type SSR, suggesting reduced complexity. Finally, our S2 cell data indicate that Past1 may activate the membrane- binding/remodeling activity of Synd.

These results suggest a novel mechanism for SSR elaboration at the wild-type NMJ involving sequential steps of membrane remodeling (Figure 7). In this model, Amph localizes and generates membrane tubules proximal to the bouton, and Past1 and Synd work together to further elaborate the tubules distal to the bouton. Successive rounds of these events could lead to the growth and expansion of layers of reticulum. In *past1* mutants, this process is severely compromised, resulting in nodules containing a core of inactive Synd packed by Amph-dependent membrane sheets.

One issue that remains to be resolved is whether direct physical interactions among Past1, Amph, and Synd (within the SSR subdomains to which they colocalize) contribute to Past1-dependent membrane remodeling at the NMJ, as they do in other systems (Xu *et al.*, 2004; Braun *et al.*, 2005; Pant *et al.*, 2009). Our S2 cell data (Figure 4) suggest that Past1 and Synd functionally interact in vivo. However, we were unable to biochemically detect Past1-Amph or Past1-Synd complexes using coprecipitation experiments in extracts from *Drosophila* larvae or S2 cells or with purified proteins (unpublished results), suggesting that either they do not directly interact or their interactions are not preserved in solution under the conditions tested. Genetic experiments at the NMJ using mutations that disrupt putative Past1-Synd and Past1-Amph interactions are unlikely to be informative because *synd* and *amph* single mutants exhibit no dramatic phenotype in SSR organization (Leventis *et al.*, 2001; Razzaq *et al.*, 2001; Zelhof *et al.*, 2001; Kumar *et al.*, 2009b), perhaps due to redundancy with other membrane-remodeling proteins. In fact, in addition to Amph and Synd, we found that the BAR proteins Cip4 and dRich are localized to nodules in *past1* mutants (Supplemental Figure S3), suggesting that multiple membrane-remodeling proteins are available to function in the Past1-dependent pathway. In the future, it will be important to build into our working model the additional roles of these and other SSR-localized membrane-remodeling proteins, as well as the timing of exocyst-dependent membrane addition (Teodoro *et al.*, 2013).

Role of Past1 in NMJ development and function

Our results demonstrate that postsynaptic Past1 plays critical roles in the structure and function of the *Drosophila* NMJ. Past1 mutant NMJs exhibit aberrant morphology and excess ghost boutons. These ghost boutons are unlikely to be due to defective clearance of excess neuronal membrane as previously described (Fuentes-Medel *et al.*, 2009), since we did not observe large amounts of neuronal debris (Figure 1H). They are also unlikely to be related to excess ghost boutons seen in Wingless (Wg) signaling pathway mutants (Ataman *et al.*, 2006, 2008), since *past1* mutants do not phenocopy many other aspects of reduced Wg signaling, including increased GluR levels, disrupted presynaptic function, and reduction in bouton number (Packard *et al.*, 2002; Speese *et al.*, 2012). The likeliest interpretation is that Past1 functions directly in SSR membrane elaboration, consistent with our EM observations, and ghost boutons may arise when membrane nodules become too severe to allow SSR assembly around boutons that form toward the end of larval development.

Another prominent synaptic phenotype that we found in *past1* mutants is a strong and specific reduction in localization of GluRIIA to postsynaptic specializations, resulting in decreased mEPSP amplitude (Figure 2). This decrease in GluRIIA could potentially arise by many mechanisms, including altered transcriptional or translational regulation or GluR traffic to or from the synapse. Indeed, expression of a dominant-negative EHD1 suppresses AMPA (α-amino-3-hydroxy-5-methyl-4-isoxazolepropionic acid–type) glutamate receptor recycling in hippocampal dendritic spines (Park *et al.*, 2004). Although there has been little evidence that *Drosophila* GluRs are regulated by membrane traffic, our data implicating the membrane-remodeling protein Past1 indicate that this may be the case. Finally, unlike the great majority of perturbations that reduce GluRIIA levels (reviewed in Frank, 2014), *past1* mutants surprisingly fail to compensate for this loss by homeostatic up-regulation of presynaptic release, suggesting that Past1 could be involved in relaying an as-yet-unidentified retrograde signal for synaptic homeostasis. Further work exploring mechanisms of GluRIIA regulation and retrograde signaling will be required to understand the role of Past1 in these events.

Our present data cannot distinguish whether the function of Past1 in GluR traffic or homeostasis is directly related to its role in SSR elaboration, and it is possible that membrane compartments independent of the SSR are required for these functions and are disrupted in the mutant. Our finding that GluRIIA levels are still reduced in *amph; past1* double mutants although SSR nodules are suppressed (Figure 6D) supports the conclusion that GluR localization defects are independent of aberrant SSR morphogenesis. Of note,

10 µm. (D) Representative traces from muscle recordings. The *x*-axis scale bar, 50 ms (EPSPs), 10,000 ms (mEPSPs); *y*-axis scale bar, 5 mV (EPSPs), 1 mV (mEPSPs). (E–H) Quantification of electrophysiological phenotypes. (E) mEPSP amplitude, (F) EPSP amplitude, (G) mEPSP frequency, and (H) quantal content, adjusted for nonlinear summation (NLS). Genotypes include *white* (wild type), $n = 31$; $past1^{60\text{-}4/110\text{-}1}$, $n = 13$; $GluRIIA^{SP16}$, $n = 44$; and $GluRIIA^{SP16}$; $past1^{60\text{-}4/110\text{-}1}$, $n = 16$.

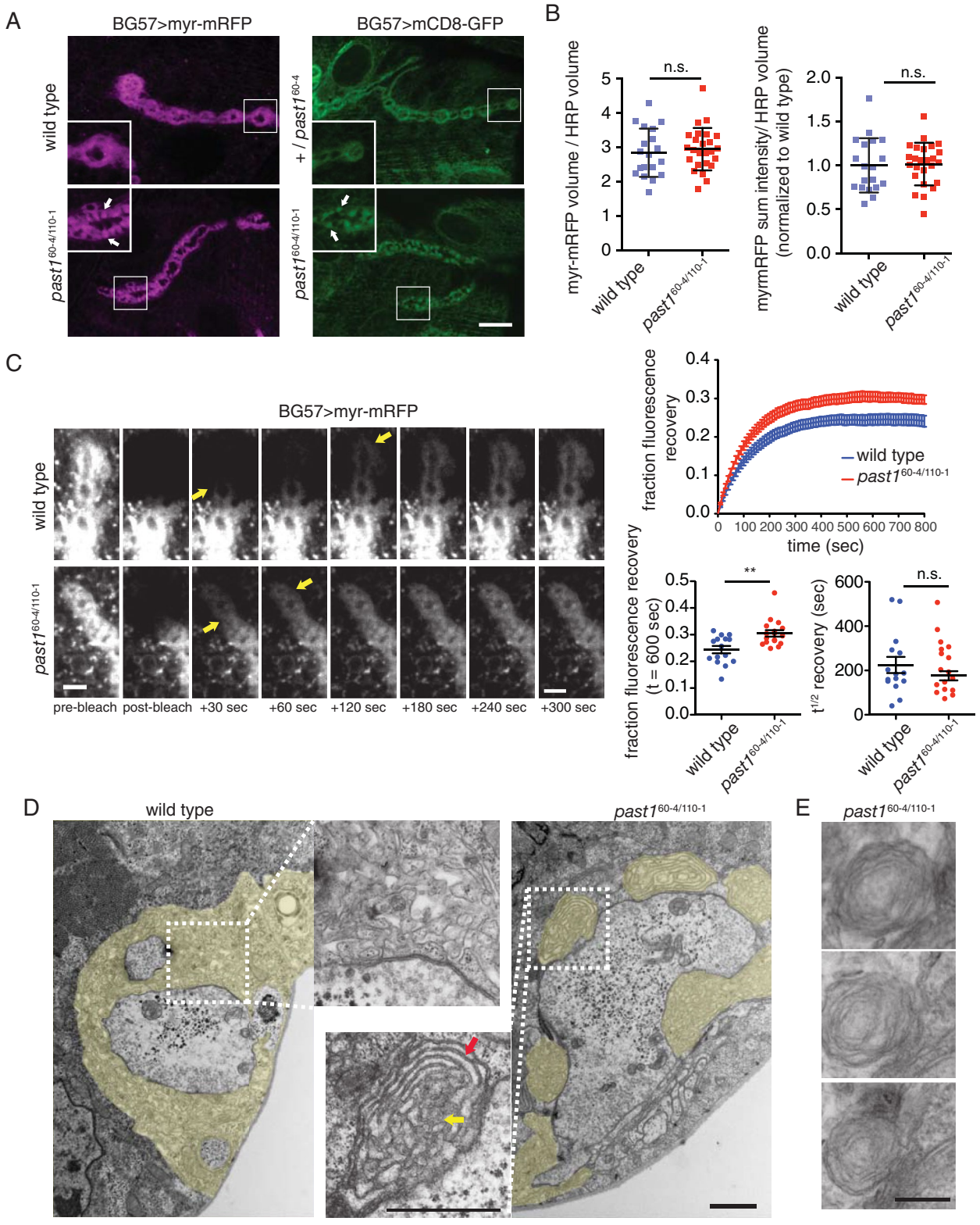

FIGURE 3: Postsynaptic membrane organization is altered in *past1* mutants. (A) Third-instar larval NMJ expressing myr-mRFP or mCD8-GFP under the control of BG57-GAL4. Images and insets show a single 100× spinning-disk confocal slice from muscle 4, segment A3. Arrows indicate postsynaptic foci. Scale bar, 10 μm. (B) Quantifications of myr-mRFP sum intensity and volume relative to HRP-labeled neuronal arbor volume. (C) Time-lapse of representative FRAP analysis of myr-mRFP turnover in wild-type and mutant larvae. A single spinning-disk 60× confocal slice from muscle 4, segment A3/A4, is shown. Arrows indicate progressive recovery of fluorescence from proximal to distal boutons. Scale bar, 5 μm. Quantification of FRAP recovery. (D) TEM of NMJs from wild-type and *past1*-mutant larvae. SSR is highlighted in yellow; red arrow indicates membrane sheets, and yellow arrow indicates membrane core. Scale bar, 1 μm. (E) *past1*-mutant NMJs exhibit membrane sheets. Three ~70-nm serial sections from a *past1*-mutant NMJ. Scale bar, 250 nm.

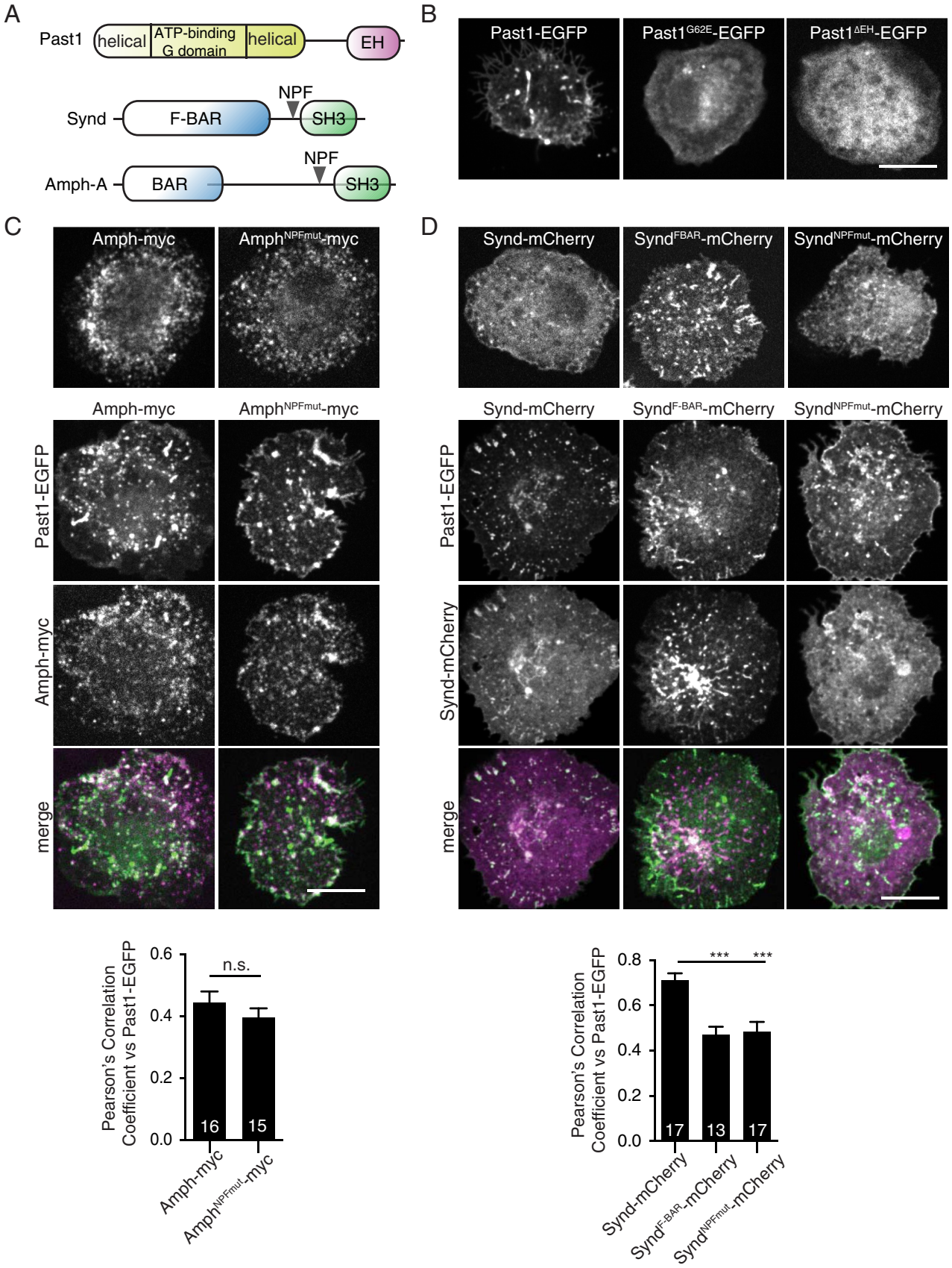

FIGURE 4: Past1, Amph, and Synd colocalization in heterologous cells. (A) Domain structure of Past1, Amph-A, and Synd. (B–D) Expression of Past1-EGFP, Synd-mCherry, and Amph-A in S2 cells spread on concanavalin A. Single 100× confocal slices ~1 µm from the cell–coverslip interface from representative cells. Bar graphs show mean Pearson's *r*; number in bar indicates number of cells measured. Scale bars, 10 µm.

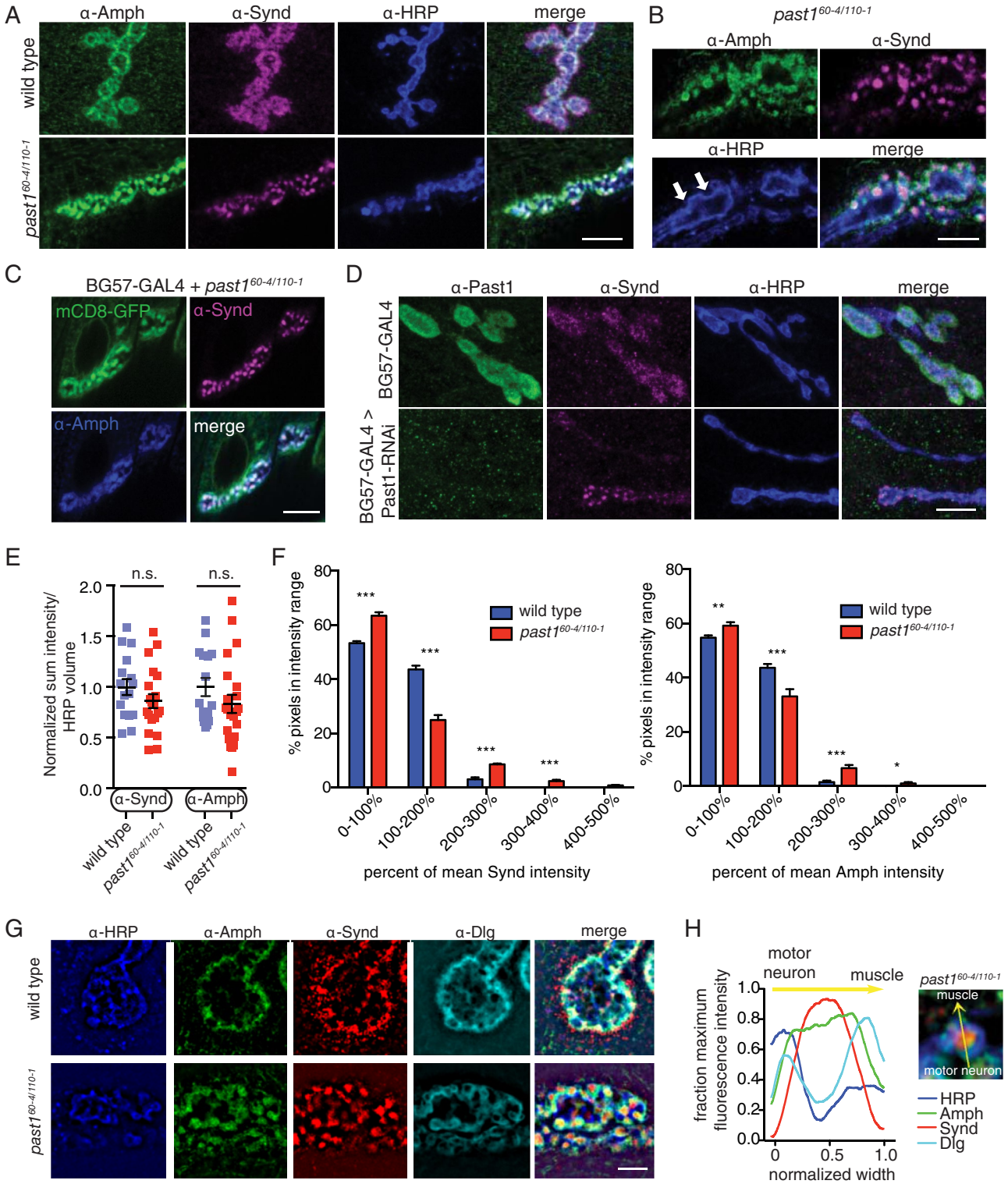

FIGURE 5: Past1 is required for postsynaptic subdomain organization of Synd and Amph. (A) Maximum intensity projections of 60× spinning-disk confocal stacks from representative muscle 4 NMJs. Scale bar, 10 μm. (B) Single 63× laser scanning confocal slice (muscle 4) showing membrane nodules adjacent to neuronal membrane indentations (arrows). Scale bar, 5 μm. (C) Localization of BG57-GAL4–driven mCD8-GFP in *past1* NMJs. A single 60× confocal slice from a representative muscle 4 is shown. Scale bar, 10 μm. (D) Nodules are recapitulated by postsynaptic *past1* RNAi. Maximum intensity projections of 60× spinning-disk confocal stacks from representative muscle 4 NMJs. Scale bar, 10 μm. (E) Quantification of Amph and Synd intensity in 3D volumes surrounding HRP-positive motor neuron. (F) Quantification of Synd and Amph nodules in *past1* NMJs. Histograms depict fraction of pixels at indicated intensities in 1.5-μm dilated area surrounding α-HRP–positive motor neuron terminal. (G) Single structured illumination slices of wild-type and *past1*-mutant NMJs. Scale bar, 2 μm. (H) Mean intensity profiles of nodules in *past1* mutants along a line traced perpendicular to the neuronal membrane (as indicated in image) and normalized to the width of the Synd peak.

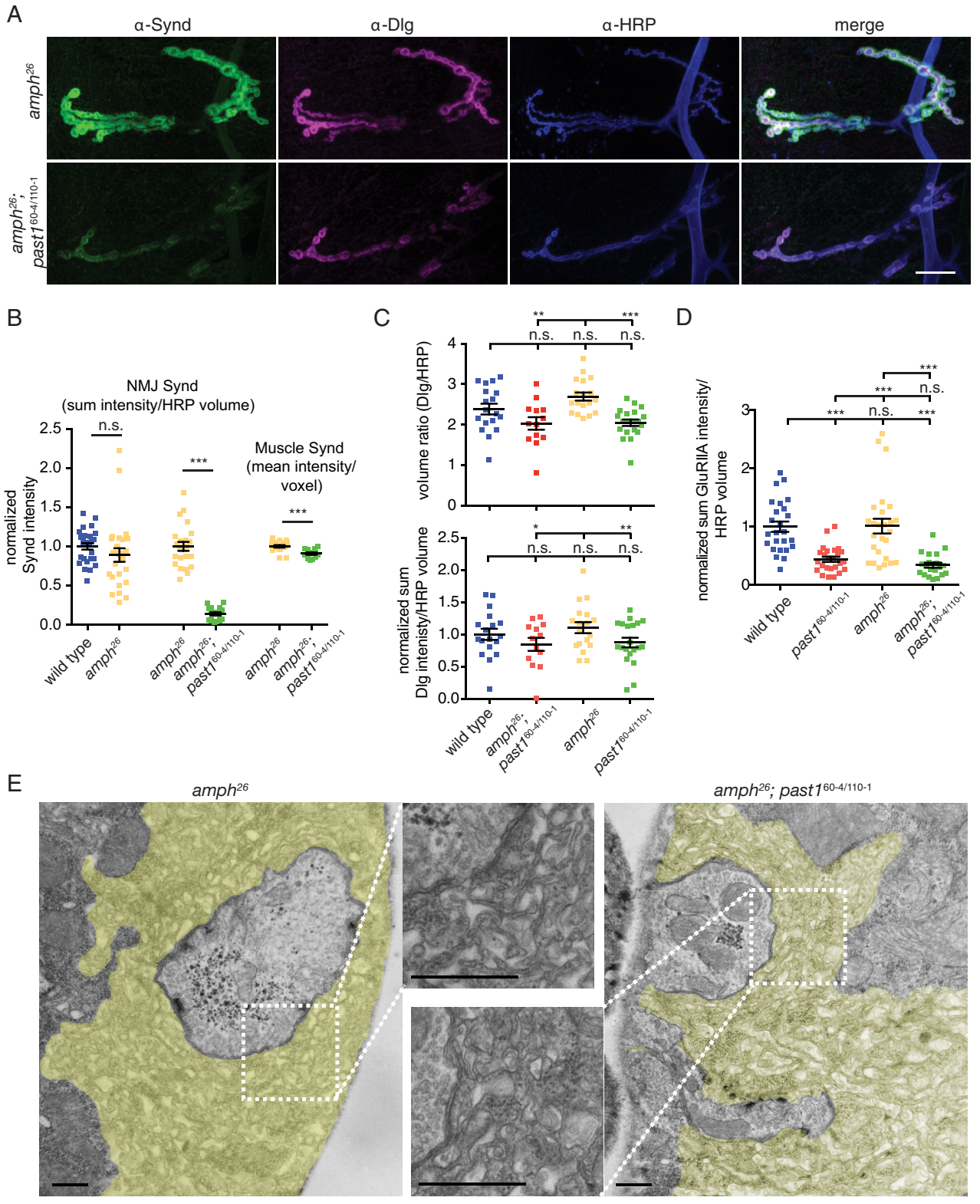

FIGURE 6: Amph is required for Synd nodule formation. (A) Synd nodules are lost in *amph; past1* double mutants. Maximum intensity projections of 100× confocal stacks from representative muscle 4 NMJs labeled with the indicated antibodies. Scale bar, 20 µm. (B) Quantification of Synd at the NMJ and in the muscle. NMJ Synd is more drastically depleted than muscle Synd. Statistical analyses represent *t* tests comparing experiments done in parallel. (C) Dlg volume and intensity are similar in *past1* and *past1*; *amph* mutants. Top, quantification of Dlg volume surrounding muscle 4, segment A3, presynaptic terminals. Bottom, quantification of Dlg intensity surrounding presynaptic terminals. (D) GluRIIA intensity is similarly reduced in *past1* and *past1*; *amph* mutants compared with wild type. Quantification of GluRIIA intensity on muscle 4, segment A3. (E) TEM of NMJs from *amph* and *amph; past1* mutant larvae. *past1* membrane nodules are suppressed by loss of *amph*. SSR is highlighted in yellow; scale bar, 500 nm.

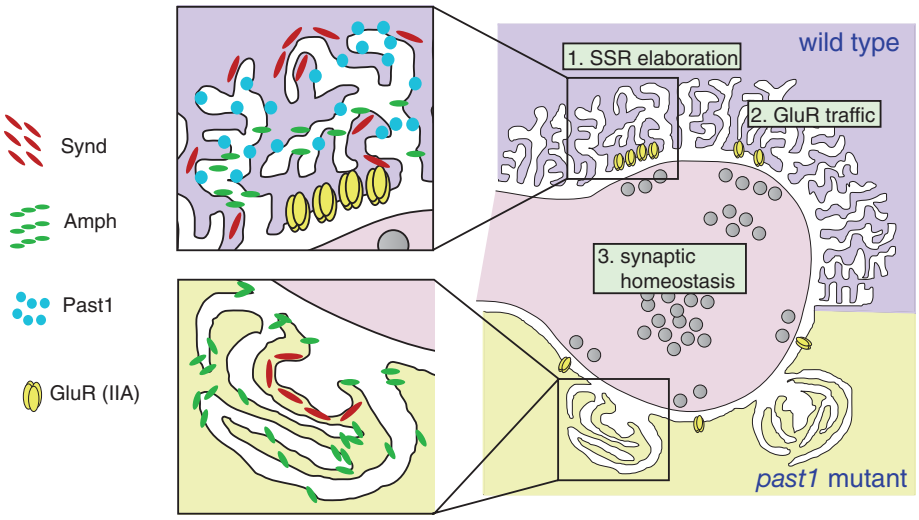

FIGURE 7: Model depicting the role of Past1 in postsynaptic membrane organization and function. In wild-type animals, sequential steps of membrane remodeling by components of the Amph membrane domain (generating sheets) and the Synd membrane domain (forming tubules from these sheets) lead to the elaboration of increasing layers of reticulum. In *past1* mutants, the Synd domain collapses into nodules that are packed in by Amph-dependent sheets.

Antibodies

α-Past1 (1:1000; Olswang-Kutz *et al.*, 2009), α-Amph (1:1000; Zelhof *et al.*, 2001), α-Synd (1:1000; Kumar *et al.*, 2009b), α-dRich (1:100; Nahm *et al.*, 2010b), and GlurIIB (1:2000) and α-GluRIIC (1:3000; Marrus *et al.*, 2004) antibodies have been described previously. Chicken α-Cip4 antibodies were obtained from N. Harden (Simon Fraser University, Burnaby, BC, Canada. (#4698, 1:1000). α-Dlg (4F3, 1:100), α-Futsch (22c10, 1:500), α-Csp, α-spectrin-α (3A9, 1:50), α-GluRIIA (8B4D2, 1:10), and α-BRP (nc82, 1:100) antibodies were obtained from the Developmental Studies Hybridoma Bank (Iowa City, IA). For double labeling of BRP and GluRIIC, antibodies were directly conjugated to Alexa 488 (α-BRP) and Alexa 546 (α-GluRIIC) (Jorquera *et al.*, 2012). Otherwise, α-HRP antibodies and secondary antibodies for imaging were conjugated to Dylight 405, Dylight 488, Rhodamine Red-X, or Alexa 647 (Jackson ImmunoResearch, West Grove, PA).

many mutants with severely defective SSR and/or reduced GluR levels exhibit normal homeostasis (e.g., *GluRIIA*, which also has reduced SSR (Petersen *et al.*, 1997; Schmid *et al.*, 2006); *Dlg* (Budnik *et al.*, 1996); *Gtaxin*, (Gorczyca *et al.*, 2007); and *Pak1* (Albin and Davis, 2004), suggesting that homeostasis is a specific function of Past1 rather than a general SSR- or GluR-related defect.

Conservation of C-terminal EHD protein function at the NMJ

Past1 represents the sole EHD homologue in *Drosophila*, whereas mammals express four EHD proteins with distinct functions (Naslavsky and Caplan, 2011). Of importance, many of the roles we defined for EHD proteins at the NMJ and in muscle are likely to be conserved. Past1 localizes to the NMJ, the muscle cortex, and myotendinous junctions (Supplemental Figure S1). However, unlike EHD1 (Posey *et al.*, 2014), Past1 does not significantly localize to t-tubules. The activities we identified for Past1 at the *Drosophila* NMJ may inform mechanisms by which EHD2 participates in sarcolemmal repair at the muscle cortex (Marg *et al.*, 2012), EHD3 functions in cardiac muscle physiology (Curran *et al.*, 2014), and EHD1 and EHD4 act at the mouse NMJ (Mate *et al.*, 2012). Our findings set the stage for uncovering how neuromuscular synapses are formed and elaborated and illustrate how cooperation between lipid-remodeling proteins can create highly complex membrane structures.

MATERIALS AND METHODS

Fly stocks

Flies were cultured using standard media and techniques. UAS-Past1-EGFP and UAS-Past1^{G62E}-EGFP lines were constructed in pBI-UASC-Gateway (Wang *et al.*, 2011) using the *PAST1*-RB transcript and inserted into the Attp40 locus (Markstein *et al.*, 2008) on *Drosophila* chromosome II at Genetic Services (Cambridge, MA). P{TRiP.HMS00557}attP2 was used for RNAi. The *past1*$^{60-4}$ and *past1*$^{110-1}$ (Olswang-Kutz *et al.*, 2009), *amph*^{26} (Razzaq *et al.*, 2001; Zelhof *et al.*, 2001), *synd*^{ex22} and *synd*^{1d} (Kumar *et al.*, 2009a), *GluRIIA*^{SP16} (Petersen *et al.*, 1997), and BG57-GAL4 and BG487-GAL4 (Budnik *et al.*, 1996) lines have been described previously.

Immunohistochemistry, imaging, and analysis of NMJ morphology

For analysis of NMJ morphology and protein localization at the NMJ, flies were cultured at controlled density at 25°C. Wandering third-instar larvae were dissected in calcium-free HL3.1 saline (Feng *et al.*, 2004) and fixed in HL3.1 containing 4% formaldehyde (or Bouin's fix for α-GlurRIIA, α-spectrin, and Cip4 staining) before antibody staining. For analysis of NMJ morphology, NMJs on muscle 6/7 and muscle 4, segment A3, were selected.

Spinning-disk confocal *Z*-stacks (0.3 μm) were collected at room temperature on an Andor spinning-disk confocal system consisting of a Nikon Ni-E upright microscope equipped with 60× (numerical aperture [NA] 1.4) and 100× (NA 1.45) oil immersion objectives, a Yokogawa CSU-W1 spinning-disk head, and an Andor iXon 897U electron-multiplying charge-coupled device camera (Andor, Belfast, Northern Ireland). Images were collected using NIS Elements AR software (Nikon, Melville, NY). Laser scanning confocal images were acquired at room temperature on a Leica SP5 confocal microscope equipped with an HCX PL APO lambda blue 63.0× (NA 1.4) oil immersion objective and Leica software (Leica, Wetzlar, Germany). SIM images were collected at room temperature on a Nikon N-SIM instrument equipped with an Apo TIRF 100× (NA 1.4) objective. Images were acquired using a violet-to-red diffraction grating at three angles and five phases of illumination, producing 15 raw images for SIM analysis using NIS Elements software.

For TEM, samples were fixed, embedded, and sectioned as previously described (Karnovsky, 1965). Sections were imaged on a JEOL 1200EX 80-kV electron microscope at 6500, 8000, or 12,000× magnification (JEOL, Peabody, MA). Data were collected from type Ib boutons, defined by their extensive SSR.

Live imaging and fluorescence recovery after photobleaching

Wandering third-instar larvae were dissected in HL3.1 saline, and the CNS was removed. Type Ib NMJs on muscle 4 were imaged on a spinning-disk confocal microscope (see earlier description) with a 60× water-dipping objective (NA 1.0). From three to 10 confocal stacks

were collected for the prebleach intensity before two to three regions/NMJ were bleached using a Mosaic 3 photoillumination device equipped with a 450-mW, 405-nm laser (Andor). Fluorescence recovery was measured by collecting confocal stacks at 10-s intervals for 450 s. *Z*-drift was corrected by manually selecting an in-focus range of confocal slices, and *XY* drift was corrected automatically using the Image registration function in NIS Elements software. Fluorescence recovery in two-dimensional (2D) projections of these confocal stacks were normalized to prebleach (1) and postbleach (0) fluorescence intensities and analyzed with GraphPad Prism (GraphPad, La Jolla, CA).

S2 Cell culture and imaging

S2 cells (Cherbas and Cherbas, 1998) were cultured according to standard protocols in Schneider's medium supplemented with 10% fetal bovine serum and 0.1 mg/ml penicillin/streptomycin. Past1-EGFP and Past1^{G62E}-EGFP were described earlier. Past1$^{\Delta EH}$-EGFP was generated by deleting sequences coding amino acids 417–534 of Past1. Synd (isoform A)-mCherry and Synd$^{F\text{-}BAR}$-mCherry (amino acids 1–300, as previously described in Becalska *et al*. 2013) were generated in pBI-UASc (Wang *et al*., 2011). Amph-A was constructed in pUAST and tagged with five copies of the myc epitope. Site-directed mutagenesis was used to generate Amph-A^{F516A} (Amph-A^{NPFmut}) and Syndapin^{F418A} (Syndapin^{NPFmut}). Constructs were cotransfected with Actin-GAL4 using Effectene reagent (Qiagen, Valencia, CA) and incubated for 2–3 d at 25°C. Cells were spread for 1 h on coverslips coated with concanavalin A (Rogers *et al*., 2003; Sigma-Aldrich, St. Louis, MO), fixed for 10 min in 4% formaldehyde in phosphate-buffered saline (PBS), and then, where indicated, permeabilized, stained with primary and secondary antibodies, and washed with PBS plus 0.1% Triton X-100. Samples were mounted in Mowiol with DABCO (Sigma-Aldrich), and cells were imaged by spinning-disk confocal microscopy as described earlier.

Electrophysiology and analysis

Wandering third-instar larvae were chosen for electrophysiology. Larvae were dissected in a modified HL3 saline: NaCl (70 mM), KCl (5 mM), $MgCl_2$ (10 mM), $NaHCO_3$ (10 mM), sucrose (115 mM = 3.9%), trehalose (4.2 mM = 0.16%), HEPES (4-(2-hydroxyethyl)-1-piperazineethanesulfonic acid; 5.0 mM = 0.12%), and $CaCl_2$ (0.5 mM). Sharp electrode recordings were taken from muscle 6 of abdominal segment A2 or A3, as previously described (Davis *et al*., 1998; Frank *et al*., 2006). Data were collected using an Axopatch 200B amplifier (Molecular Devices, Sunnyvale, CA), digitized using a Digidata 1440A data acquisition system (Molecular Devices), and recorded with pCLAMP 10 acquisition software (Molecular Devices). For presynaptic nerve stimulation, a Master-8 pulse stimulator (A.M.P. Instruments, Jerusalem, Israel) and an ISO-Flex isolation unit (A.M.P. Instruments) were used to deliver 1-ms suprathreshold stimuli to the appropriate segmental nerve. The average spontaneous miniature EPSP (mEPSP) amplitude was quantified by measuring the amplitude of ~100–200 individual spontaneous release events per NMJ. The average evoked EPSP amplitude was calculated for each NMJ. Quantal content (QC) was determined for each NMJ by calculating the ratio of average EPSP and average mEPSP amplitudes. QC was corrected for nonlinear summation as described (Martin, 1955).

Image and statistical analyses

Analyses of postsynaptic volumes and volumetric intensities were conducted using the Volocity 5.5 Classification Module (ImproVision, Waltham, MA). Volumes corresponding to presynaptic (as determined by HRP) labeling were determined using intensity thresholds, as previously described (Ramachandran *et al*., 2009). Postsynaptic areas were determined by dilating the HRP signal to include all of the quantified postsynaptic label intensity for each antigen and kept identical between control and experimental samples. Presynaptic, postsynaptic, or total (presynaptic and postsynaptic) immunolabeling intensities were normalized to total presynaptic volumes (i.e., HRP-delineated bouton volumes).

Colocalization analyses in S2 cells were conducted in single confocal slices 1–1.5 µm from the coverslip–cell interface. Pearson's *r* was calculated from background-subtracted images using the ImageJ plug-in coloc2 and Costes' randomization test (fiji.sc/Coloc_2). Synd and Amph pixel intensity distributions at the NMJ were calculated in ImageJ from sum intensity projections of confocal stacks. The α-HRP–positive presynaptic area was dilated by 1.5 µm to define the postsynaptic region. Images were then normalized to the mean Synd/Amph intensity in this area, and pixel intensity distributions were calculated using the Sixteen Bit Histogram plugin in Image-J. Data were binned as indicated and graphed using GraphPad Prism.

All errors shown are mean ± SEM. Statistical significance was calculated using GraphPad Prism software using analysis of variance followed by pairwise Tukey's tests or using Student's *t* tests where only two groups were compared; $*p < 0.05$, $**p < 0.01$, $***p < 0.005$; n.s., not significantly different.

ACKNOWLEDGMENTS

Stocks and reagents were generously provided by Aaron DiAntonio, Seungbok Lee, Andrew Zelhof, Mani Ramaswami, Mia Horowitz, Troy Littleton, the Bloomington *Drosophila* Stock Center (Bloomington, IN; National Institutes of Health P40OD018537), the *Drosophila* Genomics Resource Center (Bloomington, IN), and the Developmental Studies Hybridoma Bank (University of Iowa). We thank Bruce Goode, Troy Littleton, Daniela Nicastro, Suzanne Paradis, Neil Ritter, and ShiYu Wang for helpful discussions and technical assistance, the Electron Microscopy Facility at Harvard Medical School, and Christopher O'Connell (Nikon Instruments) for assistance with the SIM experiments. This work was supported by the National Institutes of Health/National Institute of Neurological Disorders and Stroke (DP2 NS082127 to A.A.R.; NS062738 to C.A.F.), a Pew Scholar Award (to A.A.R.), the National Science Foundation (MRI DBI-1228757), and funds from the University of Iowa Carver Trust and Carver College of Medicine (to C.A.F.).

REFERENCES

Albin SD, Davis GW (2004). Coordinating structural and functional synapse development: postsynaptic p21-activated kinase independently specifies glutamate receptor abundance and postsynaptic morphology. J Neurosci 24, 6871–6879.

Ataman B, Ashley J, Gorczyca D, Gorczyca M, Mathew D, Wichmann C, Sigrist SJ, Budnik V (2006). Nuclear trafficking of *Drosophila* Frizzled-2 during synapse development requires the PDZ protein dGRIP. Proc Natl Acad Sci USA 103, 7841–7846.

Ataman B, Ashley J, Gorczyca M, Ramachandran P, Fouquet W, Sigrist SJ, Budnik V (2008). Rapid activity-dependent modifications in synaptic structure and function require bidirectional Wnt signaling. Neuron 57, 705–718.

Becalska AN, Kelley CF, Berciu C, Stanishneva-Konovalova TB, Fu X, Wang S (2013). Formation of membrane ridges and scallops by the F-BAR protein Nervous Wreck. Mol Biol Cell 24, 2406–2418.

Braun A, Pinyol R, Dahlhaus R, Koch D, Fonarev P, Grant BD, Kessels MM, Qualmann B (2005). EHD proteins associate with syndapin I and II and such interactions play a crucial role in endosomal recycling. Mol Biol Cell 16, 3642–3658.

Budnik V, Koh YH, Guan B, Hartmann B, Hough C, Woods D, Gorczyca M (1996). Regulation of synapse structure and function by the *Drosophila* tumor suppressor gene dlg. Neuron 17, 627–640.

Cherbas L, Cherbas P (1998). Cell culture. In: In*: Drosophila*: A Practical Approach, ed. DB Roberts, Oxford, UK: Oxford University Press, 319–346.
Curran J, Makara MA, Little SC, Musa H, Liu B, Wu X, Polina I, Alecusan JS, Wright P, Li J*, et al.* (2014). EHD3-dependent endosome pathway regulates cardiac membrane excitability and physiology. Circ Res 115, 68–78.
Daumke O, Lundmark R, Vallis Y, Martens S, Butler PJ, McMahon HT (2007). Architectural and mechanistic insights into an EHD ATPase involved in membrane remodelling. Nature 449, 923–927.
Davis GW, DiAntonio A, Petersen SA, Goodman CS (1998). Postsynaptic PKA controls quantal size and reveals a retrograde signal that regulates presynaptic transmitter release in *Drosophila*. Neuron 20, 305–315.
DiAntonio A, Petersen SA, Heckmann M, Goodman CS (1999). Glutamate receptor expression regulates quantal size and quantal content at the *Drosophila* neuromuscular junction. J Neurosci 19, 3023–3032.
Feng Y, Ueda A, Wu CF (2004). A modified minimal hemolymph-like solution, HL3.1, for physiological recordings at the neuromuscular junctions of normal and mutant *Drosophila* larvae. J Neurogenet 18, 377–402.
Frank CA (2014). Homeostatic plasticity at the *Drosophila* neuromuscular junction. Neuropharmacology 78, 63–74.
Frank CA, Kennedy MJ, Goold CP, Marek KW, Davis GW (2006). Mechanisms underlying the rapid induction and sustained expression of synaptic homeostasis. Neuron 52, 663–677.
Fuentes-Medel Y, Logan MA, Ashley J, Ataman B, Budnik V, Freeman MR (2009). Glia and muscle sculpt neuromuscular arbors by engulfing destabilized synaptic boutons and shed presynaptic debris. PLoS Biol 7, e1000184.
Giridharan SS, Cai B, Vitale N, Naslavsky N, Caplan S (2013). Cooperation of MICAL-L1, syndapin2, and phosphatidic acid in tubular recycling endosome biogenesis. Mol Biol Cell 24, 1776–1790.
Gorczyca D, Ashley J, Speese S, Gherbesi N, Thomas U, Gundelfinger E, Gramates LS, Budnik V (2007). Postsynaptic membrane addition depends on the Discs-Large-interacting t-SNARE Gtaxin. J Neurosci 27, 1033–1044.
Grant B, Zhang Y, Paupard MC, Lin SX, Hall DH, Hirsh D (2001). Evidence that RME-1, a conserved *C. elegans* EH-domain protein, functions in endocytic recycling. Nat Cell Biol 3, 573–579.
Jorquera RA, Huntwork-Rodriguez S, Akbergenova Y, Cho RW, Littleton JT (2012). Complexin controls spontaneous and evoked neurotransmitter release by regulating the timing and properties of synaptotagmin activity. J Neurosci 32, 18234–18245.
Karnovsky MC (1965). A formaldehyde-glutaraldehyde fixative of high osmolarity for use in electron microscopy. J Cell Biol 27, 137A.
Kumar V, Alla SR, Krishnan KS, Ramaswami M (2009a). Syndapin is dispensable for synaptic vesicle endocytosis at the *Drosophila* larval neuromuscular junction. Mol Cell Neurosci 40, 234–241.
Kumar V, Fricke R, Bhar D, Reddy-Alla S, Krishnan KS, Bogdan S, Ramaswami M (2009b). Syndapin promotes formation of a postsynaptic membrane system in *Drosophila*. Mol Biol Cell 20, 2254–2264.
Lahey T, Gorczyca M, Jia XX, Budnik V (1994). The *Drosophila* tumor suppressor gene dlg is required for normal synaptic bouton structure. Neuron 13, 823–835.
Lee DW, Zhao X, Scarselletta S, Schweinsberg PJ, Eisenberg E, Grant BD, Greene LE (2005). ATP binding regulates oligomerization and endosome association of RME-1 family proteins. J Biol Chem 280, 17213–17220.
Leventis PA, Chow BM, Stewart BA, Iyengar B, Campos AR, Boulianne GL (2001). *Drosophila* Amphiphysin is a post-synaptic protein required for normal locomotion but not endocytosis. Traffic 2, 839–850.
Lin SX, Grant B, Hirsh D, Maxfield FR (2001). Rme-1 regulates the distribution and function of the endocytic recycling compartment in mammalian cells. Nat Cell Biol 3, 567–572.
Marg A, Schoewel V, Timmel T, Schulze A, Shah C, Daumke O, Spuler S (2012). Sarcolemmal repair is a slow process and includes EHD2. Traffic 13, 1286–1294.
Markstein M, Pitsouli C, Villalta C, Celniker SE, Perrimon N (2008). Exploiting position effects and the gypsy retrovirus insulator to engineer precisely expressed transgenes. Nat Genet 40, 476–483.
Marrus SB, Portman SL, Allen MJ, Moffat KG, DiAntonio A (2004). Differential localization of glutamate receptor subunits at the *Drosophila* neuromuscular junction. J Neurosci 24, 1406–1415.
Martin AR (1955). A further study of the statistical composition on the end-plate potential. J Physiol 130, 114–122.
Masuda M, Mochizuki N (2010). Structural characteristics of BAR domain superfamily to sculpt the membrane. Semin Cell Dev Biol 21, 391–398.
Mate SE, Van Der Meulen JH, Arya P, Bhattacharyya S, Band H, Hoffman EP (2012). Eps homology domain endosomal transport proteins differentially localize to the neuromuscular junction. Skelet Muscle 2, 19.
Mathew D, Popescu A, Budnik V (2003). *Drosophila* amphiphysin functions during synaptic Fasciclin II membrane cycling. J Neurosci 23, 10710–10716.
Nahm M, Kim S, Paik SK, Lee M, Lee S, Lee ZH, Kim J, Lee D, Bae YC (2010a). dCIP4 (*Drosophila* Cdc42-interacting protein 4) restrains synaptic growth by inhibiting the secretion of the retrograde Glass bottom boat signal. J Neurosci 30, 8138–8150.
Nahm M, Long AA, Paik SK, Kim S, Bae YC, Broadie K, Lee S (2010b). The Cdc42-selective GAP rich regulates postsynaptic development and retrograde BMP transsynaptic signaling. J Cell Biol 191, 661–675.
Naslavsky N, Caplan S (2011). EHD proteins: key conductors of endocytic transport. Trends Cell Biol 21, 122–131.
Olswang-Kutz Y, Gertel Y, Benjamin S, Sela O, Pekar O, Arama E, Steller H, Horowitz M, Segal D (2009). *Drosophila* Past1 is involved in endocytosis and is required for germline development and survival of the adult fly. J Cell Sci 122, 471–480.
Packard M, Koo ES, Gorczyca M, Sharpe J, Cumberledge S, Budnik V (2002). The *Drosophila* Wnt, wingless, provides an essential signal for pre- and postsynaptic differentiation. Cell 111, 319–330.
Pant S, Sharma M, Patel K, Caplan S, Carr CM, Grant BD (2009). AMPH-1/Amphiphysin/Bin1 functions with RME-1/Ehd1 in endocytic recycling. Nat Cell Biol 11, 1399–1410.
Park M, Penick EC, Edwards JG, Kauer JA, Ehlers MD (2004). Recycling endosomes supply AMPA receptors for LTP. Science 305, 1972–1975.
Petersen SA, Fetter RD, Noordermeer JN, Goodman CS, DiAntonio A (1997). Genetic analysis of glutamate receptors in *Drosophila* reveals a retrograde signal regulating presynaptic transmitter release. Neuron 19, 1237–1248.
Posey AD Jr, Swanson KE, Alvarez MG, Krishnan S, Earley JU, Band H, Pytel P, McNally EM, Demonbreun AR (2014). EHD1 mediates vesicle trafficking required for normal muscle growth and transverse tubule development. Dev Biol 387, 179–190.
Prokop A (2006). Organization of the efferent system and structure of neuromuscular junctions in *Drosophila*. Int Rev Neurobiol 75, 71–90.
Ramachandran P, Barria R, Ashley J, Budnik V (2009). A critical step for postsynaptic F-actin organization: regulation of Baz/Par-3 localization by aPKC and PTEN. Dev Neurobiol 69, 583–602.
Rao Y, Ma Q, Vahedi-Faridi A, Sundborger A, Pechstein A, Puchkov D, Luo L, Shupliakov O, Saenger W, Haucke V (2010). Molecular basis for SH3 domain regulation of F-BAR-mediated membrane deformation. Proc Natl Acad Sci USA 107, 8213–8218.
Razzaq A, Robinson IM, McMahon HT, Skepper JN, Su Y, Zelhof AC, Jackson AP, Gay NJ, O'Kane CJ (2001). Amphiphysin is necessary for organization of the excitation-contraction coupling machinery of muscles, but not for synaptic vesicle endocytosis in *Drosophila*. Genes Dev 15, 2967–2979.
Rogers SL, Wiedemann U, Stuurman N, Vale RD (2003). Molecular requirements for actin-based lamella formation in *Drosophila* S2 cells. J Cell Biol 162, 1079–1088.
Schmid A, Qin G, Wichmann C, Kittel RJ, Mertel S, Fouquet W, Schmidt M, Heckmann M, Sigrist SJ (2006). Non-NMDA-type glutamate receptors are essential for maturation but not for initial assembly of synapses at *Drosophila* neuromuscular junctions. J Neurosci 26, 11267–11277.
Speese SD, Ashley J, Jokhi V, Nunnari J, Barria R, Li Y, Ataman B, Koon A, Chang YT, Li Q*, et al.* (2012). Nuclear envelope budding enables large ribonucleoprotein particle export during synaptic Wnt signaling. Cell 149, 832–846.
Teodoro RO, Pekkurnaz G, Nasser A, Higashi-Kovtun ME, Balakireva M, McLachlan IG, Camonis J, Schwarz TL (2013). Ral mediates activity-dependent growth of postsynaptic membranes via recruitment of the exocyst. EMBO J 32, 2039–2055.
Thomas U, Sigrist SJ (2012). Glutamate receptors in synaptic assembly and plasticity: case studies on fly NMJs. Adv Exp Med Biol 970, 3–28.
Wang JW, Brent JR, Tomlinson A, Shneider NA, McCabe BD (2011). The ALS-associated proteins FUS and TDP-43 function together to affect *Drosophila* locomotion and life span. J Clin Invest 121, 4118–4126.
Xu Y, Shi H, Wei S, Wong SH, Hong W (2004). Mutually exclusive interactions of EHD1 with GS32 and syndapin II. Mol Membr Biol 21, 269–277.
Zelhof AC, Bao H, Hardy RW, Razzaq A, Zhang B, Doe CQ (2001). *Drosophila* Amphiphysin is implicated in protein localization and membrane morphogenesis but not in synaptic vesicle endocytosis. Development 128, 5005–5015.